ORIGINAL RESEARCH PAPER

Fuel Cells DOI: 10.1002/fuce.201300197

Online Diagnosis of PEMFC by Combining Support Vector Machine and Fluidic Model▲

Z. Li[1,2,3,*] S. Giurgea[1,2], R. Outbib[3], D. Hissel[1,2]

[1] FCLAB Research Federation, FR CNRS 3539, rue Thierry Mieg, 90010 Belfort Cedex, France
[2] FEMTO-ST (UMR CNRS 6174), ENERGY Department, UFC/UTBM, 90000 Belfort, France
[3] Laboratoire des Sciences de l'Information et des Systemes (LSIS), University of Aix-Marseille, 13397 Marseille, France

Received September 10, 2013; accepted February 05, 2014; published online March 04, 2014

Abstract

This paper deals with the online fault diagnosis of polymer electrolyte membrane fuel cell (PEMFC) stack. In the proposed approach, support vector machine (SVM) and a fluidic model are correlated to realize the diagnosis of the faults on water management. With the help of the fluidic model, health states of the stack can be identified. This procedure is then dedicated to labeling the training data, which is used to train the dimension reduction model, named Fisher discriminant analysis (FDA), and the SVM classifier. The online diagnosis can then be realized by using the trained FDA and SVM models. The proposed approach is illustrated by using the experimental data of a 20-cell PEMFC stack. The feasibility of the approach for online implementation is also affirmed.

Keywords: Fault Diagnosis, FDA, Fluidic Model, PEMFC, SVM, Water Management

1 Introduction

Fault diagnosis, especially online diagnosis, has been identified as a crucial issue in the development and application of polymer electrolyte membrane fuel cell (PEMFC) technology [1]. With an effective online diagnosis approach, an earlier fault detection can be achieved so that more serious faults can be avoided. Additionally, the diagnosis results can be supplied to the control unit, thus help adjusting the control commands [2].

Recent literatures have provided several diagnostic methods that are either based on physical models, or experimental data and knowledge [3–5]. Articles in these two aspects are respectively reviewed in Refs. [6, 7]. In these two approaches, physical model based diagnosis methods have the advantages that explicit physical significance and high genericity can be ensured, although it is often difficult to develop an accurate physical model that is suitable for the fault diagnosis of PEMFC. Furthermore, a high computational effort and vast measurements could be required, especially in the case of multi-dimensional models [5, 6, 8].

The data-driven diagnosis approaches, without the sophisticated modeling process, have attracted the interest of researchers and become a new trend in PEMFC diagnosis. It seems that this kind of approaches has the potential of being more relevant for practical applications of PEMFC. Hissel et al. [4] proposed a fuzzy diagnostic model, which is used to diagnose drying of membrane and accumulation of N_2/H_2O in the anode compartment. A neural networks model based procedure to diagnose water management faults was presented by Steiner et al. [9]. Some statistical tools were also developed for PEMFC system diagnosis. For instance, a multivariate statistical method was adopted to realize the aim of fault diagnosis by Hua et al [10]. In addition, Benouioua et al. [11] and Steiner et al. [5] introduced the signal processing tools, namely multifractal analysis and wavelet transformation, to address the diagnosis issue. Although these methods can support us some candidates, much more work is still needed to build and implement an accurate and reliable diagnostic strategy. For a practical online diagnosis, several factors must be considered and satisfied: first, the diagnostic accuracy should be high enough (more than 90% for instance). Second, the computing costs must be suitable for

▲ *Paper presented at the "Fundamentals & Developments of Fuel Cells Conference 2013 (FDFC2013)", April 16–18, 2013, Karlsruhe, Germany.*

[*] *Corresponding author, zhongliang.li@lsis.org*

an embedded system. Third, the costs of measurements should be lowered as possible [11]. To our knowledge, few available literatures have considered all these aspects.

In the framework of data-driven fault diagnosis, various pattern classification techniques have been widely applied and have shown their superiority and potentials for online implementations [2]. The common classification procedure usually proceeds in two steps: firstly an empirical classifier is established from prior knowledge and history data, which is considered as training process. Then the real time data is processed by the classifier in order to determine whether and which faults occur. It should be remarked that the pattern classification belongs to supervised learning in which the classifier is trained from training data labeled with normal and various faults. However, the reality is that historical data often contains both normal and abnormal data, and cannot be intuitively labeled with the knowledge in hand. A data labeling procedure seems to be needful in such situations (which is our case) [12].

Motivated by the aforementioned considerations, the objective of this paper is to present an online PEMFC diagnosis approach, which is based on pattern classification techniques with the data labeling procedure. Our major focus in this paper is on the most common faults that correspond to water management of PEMFC: membrane drying faults and flooding faults.

Specifically, in our paper, we try to combine a powerful classification tool, support vector machine (SVM), with a fluidic model to realize the online diagnosis. The fluidic model, which is a tool to describe the fluidic condition in air channels, is dedicated to the data labeling task. With the aid of the fluidic model, raw experimental data can be labeled with three class labels that represent the states of normal and abnormal. Then the labeled data can serve as training data for the SVM classifier. In our diagnosis process, individual cell voltages are chosen as the original variables for diagnosis, since cell voltages are sensitive to certain faults and the voltage measurements are usually less expensive than others (such as fluidic measurements). Fisher discriminant analysis (FDA), as a previous step of SVM, is used to reduce the dimension of the cell-voltage constructed vectors and extract the useful features for the SVM classifier. SVM is finally performed to realize the fault diagnosis.

The rest of this paper is organized as follows. In Section 2, the principle of the proposed approach is introduced globally. Section 3 addresses the method of data labeling, which relies on the fluidic model. Section 4 is devoted to presenting the dimension reduction method FDA and the classification method SVM. The diagnosis results of a 20-cell PEMFC stack are given in Section 5. The performance of the approach is also discussed in this section. Finally, a conclusion is drawn in Section 6.

2 Principle of the Diagnosis Approach

The proposed approach in the paper is based on data and contains three stages (see Figure 1): data labeling process, model training process, and diagnosis process. The first two processes are offline, while the third process is online.

With the help of the fluidic model, the training data can be labeled with three class labels, which represent different health states: normal state, flooding fault state, and membrane drying state.

When the labeled data is available, model training process is in consideration. The models of FDA and SVM, which are utilized for dimension reduction (feature extraction) and classification are trained respectively in this stage.

In the diagnosis process, the real-time data is processed by using the FDA and SVM models obtained in the training process. Thus, the data can be classed into three classes, and the diagnosis is realized accordingly. Notice that, although multiple variables are used in data labeling process, only cell voltages are employed in the training and diagnosis processes. Additionally, the calculation time of offline labeling process and training process does not affect the final online diagnosis time.

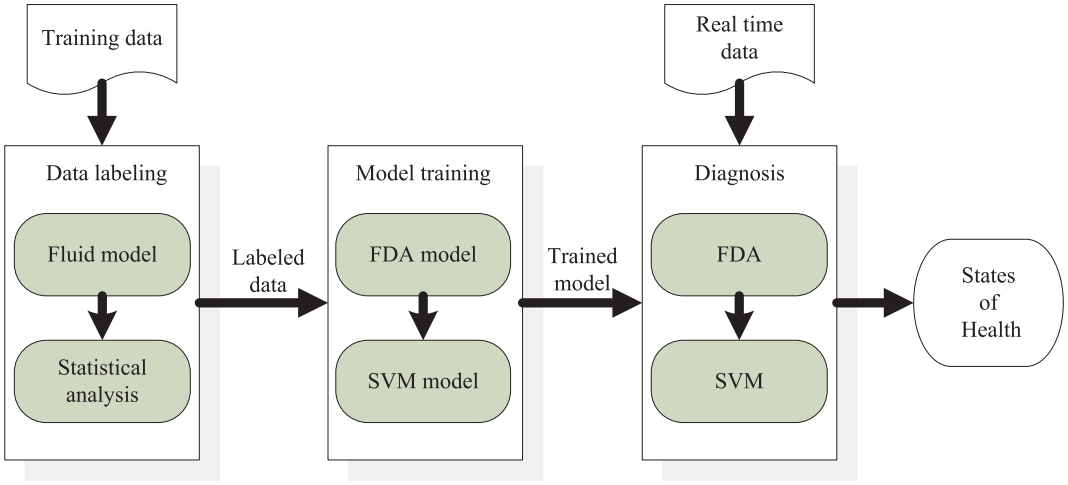

Fig. 1 Flow chart of the proposed diagnosis approach.

ORIGINAL RESEARCH PAPER

3 Data Labeling by Using Fluidic Model

In order to train the models of FDA and SVM, the training data must firstly be labeled. From the literature, fluidic model has been proven to be an efficient tool to describe the gas fluidic condition in the air channels and therefore help to identify the water management issues [13]. Thus, a fluidic model is employed to identify the concerned faults and further label the training data. In this study, the procedure is realized by comparing the real mass flow rate and theoretical mass flow rate of air.

3.1 Calculation of Real Air-Flow Rate

The average mass flow rate of air through the stack can be calculated with known variables: current I, air stoichiometry S_C, inlet air pressure P^{in}, outlet air pressure P^{out}, and relative humidity of inlet air RH^{in} (refer to [14]).

The consuming mass rate of reacted oxygen is

$$\dot{m}_{O_2}^{react} = \frac{M_{O_2} N_{cell} I}{4F} \tag{1}$$

According to ideal gas equation, the mass flow rate of inlet air and outlet air can be easily expressed, respectively, by Eqs. (2) and (3)

$$\dot{m}_{air}^{in} = S_C \dot{m}_{O_2}^{react} \frac{M_{dry\,air}^{in}}{0.21 M_{O_2}} \frac{(P^{in} - P_{H_2O}^{in}) M_{dry\,air}^{in} + P_{H_2O}^{in} M_{H_2O}}{(P^{in} - P_{H_2O}^{in}) M_{dry\,air}^{in}} \tag{2}$$

$$\dot{m}_{air}^{out} = (S_C \dot{m}_{O_2}^{react} \frac{M_{dry\,air}}{0.21 M_{O_2}} - \dot{m}_{O_2}^{react}) \times \frac{(P^{out} - P_{H_2O}^{out}) M_{dry\,air}^{out} + P_{H_2O}^{out} M_{H_2O}}{(P^{out} - P_{H_2O}^{out}) M_{dry\,air}^{out}} \tag{3}$$

Under the assumption that the relative humidity and the temperature are even over the stack, the water partial pressures $P_{H_2O}^{in}$ and $P_{H_2O}^{out}$ in the above equations are calculated by:

$$P_{H_2O}^{in} = P_{H_2O}^{out} = RH^{in} P_{sat}(T_{fc}) \tag{4}$$

where the saturation pressure is the function of temperature. In Ref. [15], the function is given by:

$$P_{sat}(T) = 1,000 \exp\left(9.3876 - \frac{3826.36}{(T - 45.47)}\right) \tag{5}$$

The molar mass of inlet dry air is

$$M_{dry\,air}^{in} = 0.21 M_{O_2} + 0.79 M_{N_2} \tag{6}$$

The molar mass of outlet dry air is calculated as

$$M_{dry\,air}^{out} = \frac{0.21(1 - (1/S_C))}{0.79 + 0.21(1 - (1/S_C))} M_{O_2} + \frac{0.79}{0.79 + 0.21(1 - (1/S_C))} M_{N_2} \tag{7}$$

From Eqs. (2) and (3), the average mass flow rate is

$$\dot{m}_{air,R}^{avg} = \frac{1}{2}(\dot{m}_{air}^{in} + \dot{m}_{air}^{out}) \tag{8}$$

Based on Eqs. (2)–(8), the average mass flow rate of air $\dot{m}_{air,R}^{avg}$ can be calculated.

3.2 Calculation of Theoretical Air-Flow Rate

In our study, the fluidic model, which is firstly proposed in Ref. [16] is employed. The model describes the air fluidic condition in a serpentine channel. With the model, the theoretical average mass flow rate $\dot{m}_{air,T}^{avg}$, which denotes the predicted normal average mass flow rate in the given condition, can be estimated.

In the model, the pressure drop in very fine channels is given by:

$$\Delta P = P^{in} - P^{out} = \frac{1}{2} \frac{(\dot{m}_{air}^{avg})^2}{A_{ch}^2 N_{ch}^2 \rho_{air}^{avg}} (\Xi + \xi) \tag{9}$$

where the frictional resistance coefficient Ξ is expressed as a piecewise function of the Reynolds number Re,

$$\Xi = \begin{cases} \frac{64 L_{ch}}{D_h Re}, & Re \le 2200 \\ 0.316 \frac{L_{ch}}{D_h} Re^{-0.26}, & Re \ge 4000 \\ \frac{L_{ch}}{D_h}(3.8991 \times 10^{-6} Re - 15.4114), & 2200 \le Re \le 4000 \end{cases} \tag{10}$$

Re is a function of the mass flow rate $\dot{m}_{air}^{avg}$ and temperature of fuel cell T_{fc} [17]:

$$Re = \frac{D_h \dot{m}_{air}^{avg} (T_{fc} + C_0)}{A_{ch} N_{ch} \mu_0 (T_0 + C_0)} \left(\frac{T_0}{T_{fc}}\right)^{1.5} \tag{11}$$

where $\mu_0 = 18.27 \times 10^{-6}$ Pa s, $C_0 = 120$ K, $T_0 = 291.15$ K.

According to the ideal gas equation, the average density of the air was computed by incorporating the flow composition and operating conditions:

$$\rho_{air}^{avg} = \frac{1}{2}\left[\frac{(P^{in} - P_{H_2O}^{in}) M_{dry\,air}^{in} + P_{H_2O}^{in} M_{H_2O}}{R T_{fc}} + \frac{(P^{out} - P_{H_2O}^{out}) M_{dry\,air}^{out} + P_{H_2O}^{out} M_{H_2O}}{R T_{fc}}\right] \tag{12}$$

In the fluidic model, the information on fuel cell geometry, such as parameters A_{ch}, L_{ch}, D_h, and N_{ch}, can be usually supported by the manufacturer. The only unknown parameter: excess bend loss coefficient ξ, is considered as a constant here and it is identified based on the data in normal state. Specifically, the term $\dot{m}_{air}^{avg}$ in Eqs. (9) and (11) is firstly substituted by $\dot{m}_{air,R}^{avg}$, which is computed by Eq. (8). Then, from Eqs. (9)–(12), ξ can be tuned by minimizing the sum square error between the computed air pressure drop and measured air pressure drop.

When ξ is obtained, in a general condition, Eqs. (9)–(12) can be seen synthetically as equations involving $\dot{m}_{air}^{avg}$. By solving the equation, the obtained answer is actually the theoretical average mass flow rate $\dot{m}_{air,T}^{avg}$. In our study, the equation is solved by means of a simple iteration method.

3.3 Identification of water management faults

As Figure 2 shows, S_C, RH^{in}, T^{fc}, P^{in}, P^{out}, and I serve as input variables. The average mass flow rate in real operation $\dot{m}^{avg}_{air,R}$ and the theoretical average mass flow rate $\dot{m}^{avg}_{air,T}$ can be calculated, respectively. In an operating fuel cell stack, other than these input variables, the quantity of water inside the stack (especially in the air channels) can impact the real mass air-flow rate $\dot{m}^{avg}_{air,R}$. Hence, the ratio between $\dot{m}^{avg}_{air,R}$ and $\dot{m}^{avg}_{air,T}$, denoted by ϕ, is used as an indicator of water management faults. The thresholds of ϕ are determined by investigating its distribution in normal state. Actually, in normal state, its deviation is due only to measurements and model errors. Consequently, with a set of normal operating data, the threshold values are then defined according to the *three-sigma rule*:

$$\phi_{max} = \bar{\phi} + 3\sigma(\phi),\ \phi_{min} = \bar{\phi} - 3\sigma(\phi) \tag{13}$$

where ϕ_{max} and ϕ_{min} are the up limit and down limit of ϕ, $\bar{\phi}$, and $\sigma(\phi)$ are respectively the mean and the standard deviation of ϕ.

When the values of ϕ follow a normal distribution in normal state (which is the case in our study), 99.73% of the values in normal state lie within three standard deviations of the mean. It can reasonably be considered that some fault occurs when ϕ goes beyond this range. Specifically, when the value of ϕ is higher than ϕ_{max}, it means that the fluidic resistance is low due to the low quantity of water inside the stack, which indicates the "membrane drying fault;" whereas, when the value of ϕ is lower than ϕ_{min}, it means that excess water inside the stack blocks the air flow, which indicates the "flooding fault."

4 Diagnosis Strategy Based on Pattern Classification

After the labeled training data is acquired, individual cell voltages are chosen as the original variables for classification in consideration of the rich information in the voltage signals and their distributions. At a time point, cell voltages are simply constituted as a vector whose dimension equals to the number of cells. The stacks developed for the high-power output applications, such as electric vehicles, are usually composed by a number of fuel cells (tens to hundreds). The technique FDA is therefore used firstly to reduce the dimensions of raw data to lighten computing costs. Moreover, by using FDA, the effective features, which are serviceable for SVM classification could be extracted from the raw data. In the feature space generated by using FDA, SVM is subsequently carried out to realize the final diagnosis.

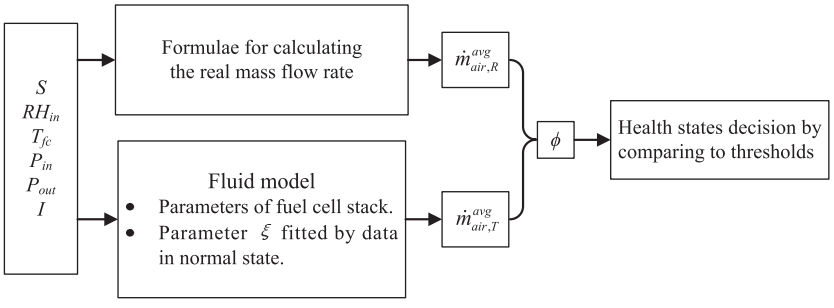

Fig. 2 Flow chart of the data labeling procedure.

4.1 Reduction of Data Dimension

For pattern recognition problems, too large dimension data can cause the so-called curse of dimensionality [18]. This will not only increase the computational complexity, but also decrease the performance [19]. Various techniques have been developed for reducing the dimensionality of the feature space in the hope of obtaining a more manageable problem [20]. FDA is such a technique whose goal is to project the original high-dimension samples to a lower-dimension space, in which the samples in the same class are concentrated, while those in different classes are separated as possible.

The FDA algorithm can be described as follows: suppose that we have a set of N H-dimensional samples $\boldsymbol{x}_1, \boldsymbol{x}_2, ..., \boldsymbol{x}_N$, which are distributed in C classes $\omega_1, \omega_2, .. , \omega_C$. The sample number in ω_i is N_i. If the original samples are supposed to be projected to a L-dimension space ($L < H$), the objective of the training process is to find H-dimension unit projecting vectors: $\boldsymbol{w}_1, \boldsymbol{w}_2, .. , \boldsymbol{w}_L$. With these vectors, a real time H-dimension sample $\boldsymbol{x}$ can be projected to the L-dimension feature space in the FDA performing process. The L-dimension projected vector $\boldsymbol{z}$ can be expressed:

$$\boldsymbol{z} = [\boldsymbol{w}_1^T\boldsymbol{x}, \boldsymbol{w}_2^T\boldsymbol{x}, \ldots, \boldsymbol{w}_L^T\boldsymbol{x}]^T \tag{14}$$

To obtain $\boldsymbol{w}_1, \boldsymbol{w}_2, ... , \boldsymbol{w}_L$, the within class matrix $\boldsymbol{S}_w$ and between class matrix $\boldsymbol{S}_b$ are defined as follows:

$$\mathbf{S}_w = \sum_{i=1}^{C}\sum_{\boldsymbol{x}_n\in\omega_i}(\boldsymbol{x}_n - \bar{\boldsymbol{x}}_i)(\boldsymbol{x}_n - \bar{\boldsymbol{x}}_i)^T \tag{15}$$

$$\boldsymbol{S}_b = \sum_{i=1}^{C} N_i(\mathbf{x}_i - \bar{\boldsymbol{x}})(\bar{\boldsymbol{x}}_i - \bar{\boldsymbol{x}})^T \tag{16}$$

where $\bar{\boldsymbol{x}}_i$ is the mean vector of class ω_i

$$\bar{\boldsymbol{x}}_i = \frac{1}{N_i}\sum_{tf="PS_iOBI"\boldsymbol{x}_n\in\omega_i}\boldsymbol{x}_n \tag{17}$$

$\mathbf{x}$ is the total mean vector

$$\bar{\boldsymbol{x}} = \frac{1}{N}\sum_{n=1}^{N}\boldsymbol{x}_n \tag{18}$$

It is proven that the optimal projecting vectors $\boldsymbol{w}_1, \boldsymbol{w}_2, ... , \boldsymbol{w}_L$ in FDA are the generalized eigenvectors of $\mathbf{S}_w^{-1}\mathbf{S}_b$ that correspond to the L largest nonzero eigenvalues. In FDA, no more than $C - 1$ of the eigenvalues are nonzero [18]. In other words, the maximum dimensional number of the feature space is $C - 1$.

ORIGINAL RESEARCH PAPER

4.2 Classification by SVM

SVM has attracted a lot of attention in the fault diagnosis domain in recent years [21]. Its remarkable characteristics, such as good generalization performance, the absence of local minima and the sparse representation of solution, make it an attractive and preferential pattern classification tool [20].

The basic theory of SVM is coming from the binary classification problem. As Figure 3 shows, there are 2-class data, which are labeled by "+1" or "-1." Suppose we have some hyperplane, which separates the points. The margin is defined as the sum of the distances from the separating hyperplane to the closest points of the two classes. SVM simply looks for the separating hyperplane with the largest margin. Support vectors (SVs) are the points that lie on the maximum margin hyperplanes. Normally, the optimal separating hyperplane is decided just by the SVs.

Specifically, suppose we have N L-dimension samples z_1, z_2, ... , z_N, which are in two classes. $g_n \in \{-1, 1\}$ is the class label of z_n. The training of SVM can be converted to solve the following quadratic problem (QP) [22]:

$$\min J(a) = \frac{1}{2}\sum_{n=1}^{N}\sum_{m=1}^{N} a_n a_m g_n g_m k(\mathbf{z}_n, \mathbf{z}_m) - \sum_{n=1}^{N} a_n \tag{19}$$

subject to

$$\sum_{n=1}^{N} a_n g_n = 0, \quad 0 \le a_n \le D, \quad \text{for} \quad n = 1, 2, \ldots, N \tag{20}$$

where $\boldsymbol{a} = [a_1, a_2, \ldots, a_N]^T$, $\{a_n\}$ are Lagrange multipliers, D is a pre-established constant, $k(z_n, z_m)$ is the kernel function of z_n and z_m, which corresponds to nonlinear mappings and takes different forms [23]. A representative kernel function, Gaussian kernel function, is utilized in the paper:

$$k(\mathbf{z}_i, \mathbf{z}_j) = \exp\left(-\frac{||z_i - z_j||^2}{\sigma}\right) \tag{21}$$

where σ is a constant that needs to be initialized.

After solving the QP problem in Eqs. (19) and (20), the samples corresponding to $a_n > 0$ are SVs, which are denoted as z_1^s, z_2^s, ... , z_S^s. The corresponding a_n and g_n are denoted by a_n^s and g_n^s. The SVs and the corresponding parameters need to be saved for the performing process.

When performing SVM, the label g of a real time sample $\boldsymbol{z}$ is calculated as

$$g = \text{sign}\left\{\sum_{n=1}^{S} a_n^s g_n^s k(z_n^s, z) + b\right\} \tag{22}$$

where

$$b = \frac{1}{S}\sum_{j=1}^{S}\left(g_j^s - \sum_{n=1}^{S} a_n^s g_n^s k(z_n^s, z_j^s)\right) \tag{23}$$

In this study, a practical approach sequential minimal optimization (SMO) is used to solve the QP problem of Eq. (19), whose details can be found in Ref. [24]. To extend the binary classifier to multi-classification situations, a method named "One-Against-One" is adopted in the paper. To train a C-class SVM, this method constructs $C(C - 1)$ classifiers, of which each one is trained on the data from two classes using binary SVM. The final classification is obtained by voting all binary classification results. The details can be found in Ref. [25].

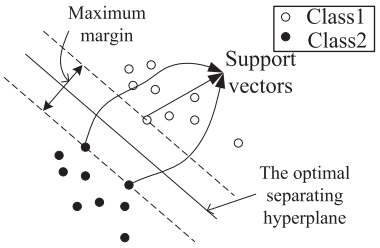

Fig. 3 Schematic diagram of the binary SVM classification.

Remarks:

(1) Although the computation seems to be complex for training the FDA and SVM model, the practical performing processes of FDA and SVM are easy to implement.

(2) There are various dimension reduction and classification methods other than FDA and SVM. Comparing with several other methods, FDA and SVM are chosen in our study in consideration of their good real-time performance and high diagnosis accuracy.

5 Results and Discussion

5.1 Experiments Presentation

A 1 kW test bench was established in the lab to test a 20-cell PEMFC stack (see Figure 4). In the test bench, a number of physical parameters impacting or expressing stack performances can be controlled and monitored. Stack temperature, hydrogen stoichiometry, air stoichiometry, relative humidity of the inlet air, and load current can be set. Inlet and outlet pressures of hydrogen and air, stack temperatures, stack voltage, and single cell voltages (denoted by $v(1)$, $v(2)$,. .. , $v(20)$)

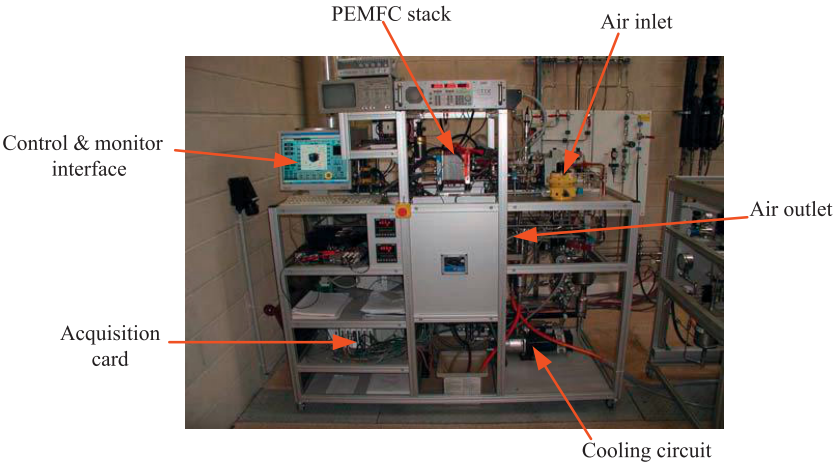

Fig. 4 Test bench.

can be monitored. The sample time of the test data is 150 ms. Additional details about the test bench and the test protocol have been previously published in Ref. [26]. Table 1 summarizes some parameters of the investigated stack.

5.2 Diagnosis Results

The experiments of normal state were firstly carried out to tune parameter ξ in Eq. (9) and define the thresholds of ϕ. In the experiments, the load current was configured in a range of values (see Figure 5). Parameter ξ is tuned by using the collected samples. By substituting the calculated values of real mass flow rate $\dot{m}^{avg}_{air,R}$ to the terms $\dot{m}^{avg}_{air}$ in Eqs. (9) and (11), the air pressure drop ΔP can be expressed as a function of ξ. With the unconstrained nonlinear optimization function "fminunc" in the Matlab optimization toolbox, ξ can then be tuned by minimizing the sum square error between the computed and measured air pressure drops.

The optimal value of ξ is 5.494, which is in accordance with the empirical values given in Ref. [16]. The *root mean squared error* statistics is 3.3662×10^{-4} between the values of computed and measured air pressure drops, which means that the model is well fitted in our case.

With the obtained ξ, $\dot{m}^{avg}_{air,T}$ can be calculated from Eqs. (9)–(12) by iteration. Figure 6 shows the computed values of $\dot{m}^{avg}_{air,R}$ and $\dot{m}^{avg}_{air,T}$ in normal state. It can be seen intuitively that the theoretical and the real mass flow rates are accordant.

The ratio ϕ between $\dot{m}^{avg}_{air,R}$ and $\dot{m}^{avg}_{air,T}$ is calculated by using the normal dataset. The thresholds of ϕ are then evaluated using the *three-sigma rule* as explained in Eq. (13). After computation, the up limit ϕ_{max} and down limit ϕ_{min} are respectively set as 1.04 and 0.96.

In order to generate the data for training and testing the FDA and SVM models, experiments about the concerning faults were also carried. In one "fault" experiment, the fuel cell stack was designed to go through "drying state," "normal state," and "flooding state." Specifically, the drying was firstly caused by starting the air circuit before adding the load. During this period, the inside water was expelled while no water was generated. Hence, the necessary water environment cannot be established, which makes the stack appear as "drying state." After a constant load was added (40 A), the relative humidity of inlet air RH^{in} was set a high level (from 85 to 110%, RH^{in} is higher than 100% which means the presence of liquid water). As liquid water accumulated, the stack went from "drying state" to "normal state," and then from "normal state" to "flooding state" successively.

The values of ϕ in the "fault" experiments are calculated and compared with ϕ_{max} and ϕ_{min}, and the states of the samples can therefore be identified. The samples can then be labeled with three class labels: "drying," "normal," and "flooding." The values of ϕ in a "fault" experiment and the labeling results can be seen in Figure 7.

Table 1 Parameters of the investigated fuel cell stack.

Parameter	Value
Cell area	100 cm^2
Cell number	20
Air channel structure	Multi serpentine
Nominal output power	500 W
Nominal operating temperature	50 °C
Operating temperature region	20–65 °C
Maximum operating pressures	1.5 bar
Anode stoichiometry	2
Cathode stoichiometry	4

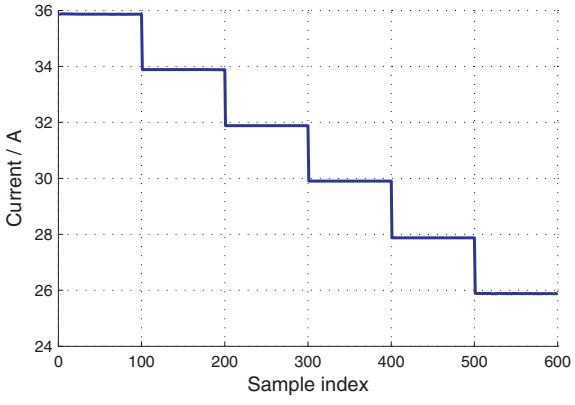

Fig. 5 Load current configuration in experiments in normal state.

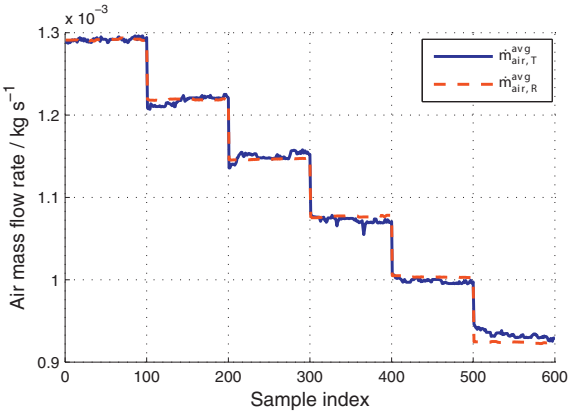

Fig. 6 Theoretical and real mass flow rates of air in normal state.

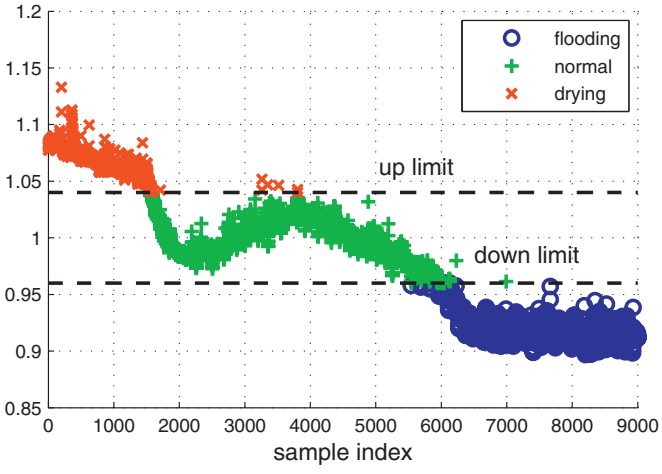

Fig. 7 Values of ϕ in fault experiment and the limits of ϕ.

After the labeling process, the labeled data from one of the "fault" experiments was used to train the FDA and SVM models. Here, individual cell voltages were selected as the original variables for the procedure. At each time point, a 20-dimension vector was constructed by 20 corresponding cell voltages.

The 20-dimension vectors were firstly used to train the FDA model. With the FDA model, the 20-dimension samples were projected to the two-dimension feature space. Figure 8 shows the projected results of the labeled training data in the two-dimension feature space. From this figure, it can be observed that the points of the identical class are concentrated, while those in the different classes are dispersive. This character of the FDA result would facilitate the classification in the following classification step.

In the feature space, the SVM model was trained to obtain a classifier. In the SVM training process, parameters D in Eq. (20) and σ in Eq. (21) are initialed after several attempts to get a relatively higher classification accuracy. After training SVM in the feature space, the optimal hyperplanes between classes were acquired. Actually, they are decided by 72 SVs and corresponding coefficients (the number of total training samples is 9,000). With the trained SVM model, any point in the feature space can be classified to one of the predefined classes. Thus, the feature space can be divided into three zones that denote the corresponding classes (see Figure 9).

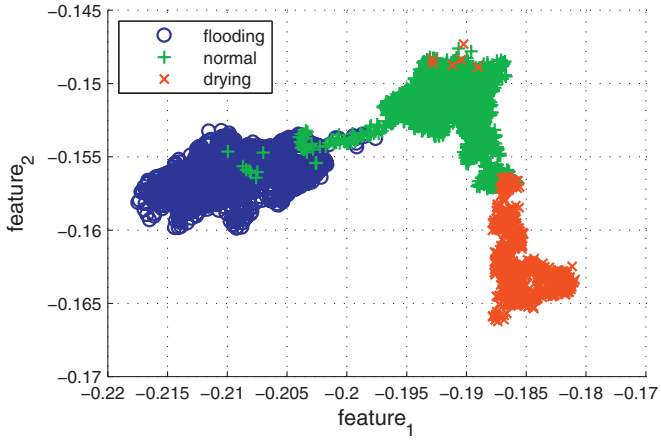

Fig. 8 Distribution of training data in feature space.

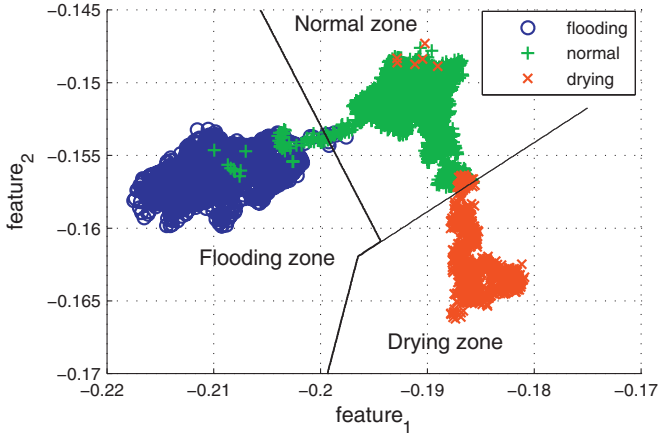

Fig. 9 Three zones divided by SVM in feature space.

5.3 Evaluation of the Performance

To evaluate the performance of the proposed approach for online application, two aspects are considered: diagnosis accuracy and computation costs.

5.3.1 Diagnosis Accuracy

It is considered that the labeling process can supply the completely correct labeling results. The error diagnosed points therefore refer to the ones whose diagnostic results are conflicting with the labeling results. To evaluate how accurately the diagnostic approach will perform in practice, an index *error diagnosis rate* (EDR) is defined. EDR means the proportion of error diagnosis points in the total data points.

In order to evaluate the generalization ability of the proposed approach, the data from another experiment other than the training data, is considered as test data. The test dataset is constituted by 10,000 labeled samples, in which the sample numbers in the drying state, normal state, and flooding state are respectively, 2063, 5712, and 2225. The EDRs of both the training data and the test data are calculated. The values are respectively 1.33 and 4.34%, which shows a globally high diagnosis accuracy. The confusion matrix of test dataset is shown in Table 2 (in the form of percentages). Over 90% of samples in each class could be diagnosed correctly, and a slight overlapping occurs between the normal state and the faulty states.

5.3.2 Computation Costs

To implement our approach, the projecting vectors in FDA procedure ($\boldsymbol{w}_1$, $\boldsymbol{w}_2$, ... , $\boldsymbol{w}_L$, here L = 2), the SVs ($\mathbf{z}_1^s$, $\mathbf{z}_2^s$, ... ,$\mathbf{z}_S^s$), and corresponding coefficients (a_n^s and g_n^s), the parameters σ in Eq. (21) and b in Eq. (22) need to be saved. In our case, 258 float numbers are in consideration. To save these numbers, less than 1 k of 16 bit memory is needed. This can be satisfied easily by the on-chip memory of a digital signal processor (DSP).

For one diagnosis procedure (to run once of FDA and SVM programs), 256 times multiplication operations, 182 times addition operations, and 72 exponent arithmetic operations are needed. These operations can be done easily by DSP in a sampling period (150 ms). Hence, it is feasible to implement the proposed approach for online diagnosis.

Table 2 Confusion matrix of the test dataset.

	Drying state (diagnosed)	Normal state (diagnosed)	Flooding state (diagnosed)
Drying state (labeled)	94.72%	5.28%	0
Normal state (labeled)	0.11%	97.18%	2.71%
Flooding state (labeled)	0	7.37%	92.63%

Table 3 Diagnostic results obtained by using SVM with FDA and without FDA.

Methods	EDR of training data	EDR of test data	Number of SVs	Needed memory	Computing time (10,000 times)
Original + SVM	0.44%	14.11%	48	1010 Floating numbers	0.1411 s
FDA + SVM	1.33%	4.34%	72	258 Floating numbers	0.0434 s

5.4 Discussion

5.4.1 The Necessity of FDA Procedure

To study the effects of FDA procedure in the diagnosis approach, the SVM was conducted directly using the cell voltages as input variables. The results obtained by using SVM with FDA as pre-procedure (FDA + SVM), and without FDA (Original + SVM) are given in Table 3. It is shown that, although a lower EDR on training data can be got by using Original + SVM than by using FDA + SVM, the EDR on test data using Original + SVM is much higher. Since the EDR on test data is usually our concern, a higher diagnosis accuracy could be obtained by using FDA + SVM. It could also be inferred that FDA + SVM has better generalization ability. With regards to the computation costs, less SVs are obtained from training Original + SVM than ones from training FDA + SVM. Nevertheless, the smaller needed memory and the shorter computing time make the approach FDA + SVM more competitive than the other one. Hence, using FDA as a pre-procedure of SVM could get the benefits in both the diagnosis accuracy and the computation cost in our case.

It should be noticed that whether it is relevant is determined essentially by the nature of the classification problem, such as the number of classes (states), the degree of overlapping, and of course the original data dimension (cell number). Although FDA plays an important role in our case, it is still recommended that the designers compare the performances of the algorithms with and without FDA carefully (as what we did in the paper) before the decision of the final diagnostic strategy.

5.4.2 The Impacts of the Fuel Cell Number

The experimental data from a 20-cell stack was used to verify the algorithms in the study. When we deal with the stacks with the different numbers of fuel cells, the efficiency of the proposed approach should be evaluated. Normally, the larger the fuel cell number is, the more information could be drawn from the cell voltages for diagnosis. It could therefore be roughly induced that the approach could be effective when the fuel cell number is equal or bigger than 20. As the stacks with less fuel cells are handled, the efficiency of the approach might be degraded. For instance, when the extreme case of one fuel cell is considered, we can imagine that the diagnosis accuracy should be low, for little diagnosis oriented information could be extracted from one-dimensional data. However, it is hard to tell a specific fuel cell number below which the approach becomes unacceptable, unless the corresponding experimental data of the stacks with various cell numbers is available. Since the approach is data based, it is desirable that the approach is tested and evaluated offline when a specific case is confronted.

6 Conclusion

In this paper, an online diagnosis approach related to water management issues in a PEMFC stack is proposed. The approach is realized combining FDA and SVM pattern recognition methods and a fluidic model.

From the results of a 20-cell fuel cell stack, several conclusions can be drawn: first, with the help of the fluidic model, flooding and membrane drying faults can be identified, and this procedure can be used to label the raw experiment data. Second, cell voltages can serve as diagnosis variables for the concerned faults. Third, by using trained FDA and SVM on cell voltages constructed vectors, the concerned faults can be detected with a high accuracy. Fourth, the computation costs of the approach are demonstrated to be suitable for online implementation. All these conclusions make the proposed diagnosis approach a promising online diagnosis tool. At present, the work of embedded coding and online test has been started in our lab.

Currently, the approach is employed only for detection of water management faults. From some experiment results, it is observed that cell voltage signals are also sensitive to some other faults of PEMFC stack, such as CO poisoning on the anode side. Hence, it is possible to extend this approach to the detection of other faults and fault isolation by increasing the number of classes and the training data related to the corresponding faults. This work is in progress in our lab.

It should be remarked that the application of pattern recognition or machine learning techniques to the fault diagnosis domain, especially to the diagnosis of PEMFC is still in its early stage. In the future, great efforts should be made to address, for instance, the fault diagnosis of PEMFC in high dynamic process.

Acknowledgment

This Ph.D. work is a contribution to the ANR DIAPASON2 project (fuel cell diagnosis methods for vehicle and stationary applications 2nd phase).

List of Symbols

a_n	Lagrange multipliers in SVM
A_{ch}	the area of channel cross section / m^2
b	bias parameter of SVM
C	number of classes
C_0	Sutherland's constant
D	pre-established constant for training SVM
D_h	hydraulic diameter / m
F	Faraday constant, 96 485.3365 / s A mol^{-1}

g	class label in binary SVM
H	dimension of original samples
I	load current / A
L	dimension of feature space
L_{ch}	length of channel / m
$\dot{m}$	mass flow rate of air / kg s^{-1}
M	molar mass / kg mol^{-1}
N	number of training samples
N_{cell}	number of fuel cells
N_{ch}	total number of the channels in stack
R	gas constant, 8.314 / J mol^{-1} K^{-1}
P	pressure / Pa
Re	Reynolds number
RH	relative humidity
S	number of support vectors
S_C	the stoichiometry factor on the cathode side
$\mathbf{S}_b$	between class scatter matrix
$\mathbf{S}_w$	within class scatter matrix
T	temperature / K
T_0	reference temperature / K
$\boldsymbol{w}$	projecting vector
$\boldsymbol{x}$	H-dimension original vector
$\boldsymbol{z}$	L-dimension projected vector in feature space

Greek Letters

Δ	variation
ω	set of the samples in one class
ϕ	ratio between real and theoretical air mass flow rates
ρ	density / kg m^{-3}
Ξ	frictional resistance coefficient
ξ	excess bend loss coefficient
σ	constant in Gaussian kernel function
μ_0	reference viscosity / Pa s

Subscript

air	humidified air
dry air	dry air
fc	fuel cell
H_2O	water
N_2	nitrogen
O_2	oxygen
R	real
sat	saturation
T	theoretical

Superscript

avg	average
in	inlet
out	outlet
react	reacted
s	support vector

Reference

[1] R. Onanena, L. Oukhellou, D. Candusso, F. Harel, D. Hissel, P. Aknin, *Int. J. Hydrogen Energy* **2010**, *33*, 2.
[2] R. Isermann, *Fault-Diagnosis Applications*, Springer, Berlin/Heidelberg, Germany, **2011**.
[3] T. Escobet, D. Feroldi, S. De Lira, V. Puig, J. Quevedo, J. Riera, M. Serra, *J. Power Sources* **2009**, *192*, 216.
[4] D. Hissel, M. C. Péra, J. M. Kauffmann, *J. Power Sources* **2004**, *128*, 239.
[5] N. Y. Steiner, D. Hissel, P. Moçotéguy, D. Candusso, *Int. J. Hydrogen Energy* **2011**, *36*, 740.
[6] R. Petrone, Z. Zheng, D. Hissel, M. C. Péra, C. Pianese, M. Sorrentino, M. Becherif, N. Y. Steiner, *Int. J. Hydrogen Energy* **2013**, *38*, 7077.
[7] Z. Zheng, R. Petrone, M. C. Péra, D. Hissel, M. Becherif, C. Pianese, N. Y. Steiner, M. Sorrentino, *Int. J. Hydrogen Energy* **2013**, *38*, 8914.
[8] S. X. Ding, *Model-Based Fault Diagnosis Techniques*, Springer, Berlin/Heidelberg, Germany, **2008**.
[9] N. Y. Steiner, D. Hissel, P. Moçotéguy, D. Candusso, *Int. J. Hydrogen Energy* **2011**, *36*, 3067.
[10] J. Hua, J. Li, M. Ouyang, L. Lu, L. Xu, *Int. J. Hydrogen Energy* **2011**, *36*, 9896.
[11] D. Benouioua, D. Candusso, F. Harel, L. Oukhellou, *Int. J. Hydrogen Energy* **2013**, *33*, 1.
[12] Q. P. He, S. J. Qin, J. Wang, *AIChE J.* **2005**, *51*, 555.
[13] S. Giurgea, R. Tirnovan, D. Hissel, R. Outbib, *Int. J. Hydrogen Energy* **2013**, *38*, 4689.
[14] R. Tirnovan, S. Giurgea, *Int. J. Hydrogen Energy* **2012**, *37*, 7745.
[15] J. Larminie, A. Dicks, M. S. McDonald, *Fuel Cell Systems Explained*, Wiley, Chichester, United Kingdom, **2003**.
[16] W. Peiyi, W. A. Little, *Cryogenics* **1983**, *23*, 273.
[17] J. R. Welty, C. E. Wicks, G. Rorrer, R. E. Wilson, *Fundamentals of Momentum, Heat, and Mass Transfer*, John Wiley & Sons, New York, USA, **2009**.
[18] C. M. Bishop, N. M. Nasrabadi, *Pattern Recognition and Machine Learning*, Springer, New York, USA, **2006**.
[19] K. Feng, Z. Jiang, W. He, B. Ma, *Expert Syst. Appl.* **2011**, *38*, 12721.
[20] L. J. Cao, K. S. Chua, W. K. Chong, H. P. Lee, Q. M. Gu, *Neurocomputing* **2003**, *55*, 321.
[21] L. Maria, R. Baccarini, V. Vieira, B. R. De Menezes, *Expert Syst. Appl.* **2011**, *38*, 6980.
[22] C. J. C. Burges, *Data Mining Knowl. Discov.* **1998**, *2*, 121.
[23] A. Widodo, B. Yang, *Mech. Syst. Signal Process.* **2007**, *21*, 2560.
[24] B. Schölkopf, C. J. C. Burges, A. J. Smola, *Advances in Kernel Methods: Support Vector Learning*, The MIT Press, Cambridge, MA, USA, **1999**.
[25] C. Hsu, C. Lin, *IEEE Trans. Neural Netw.* **2002**, *13*, 415.
[26] D. Candusso, A. De Bernardinis, M. C. Péra, F. Harel, X. François, D. Hissel, G. Coquery, J. M. Kauffmann, *Energy Convers. Manage.* **2008**, *49*, 880.

